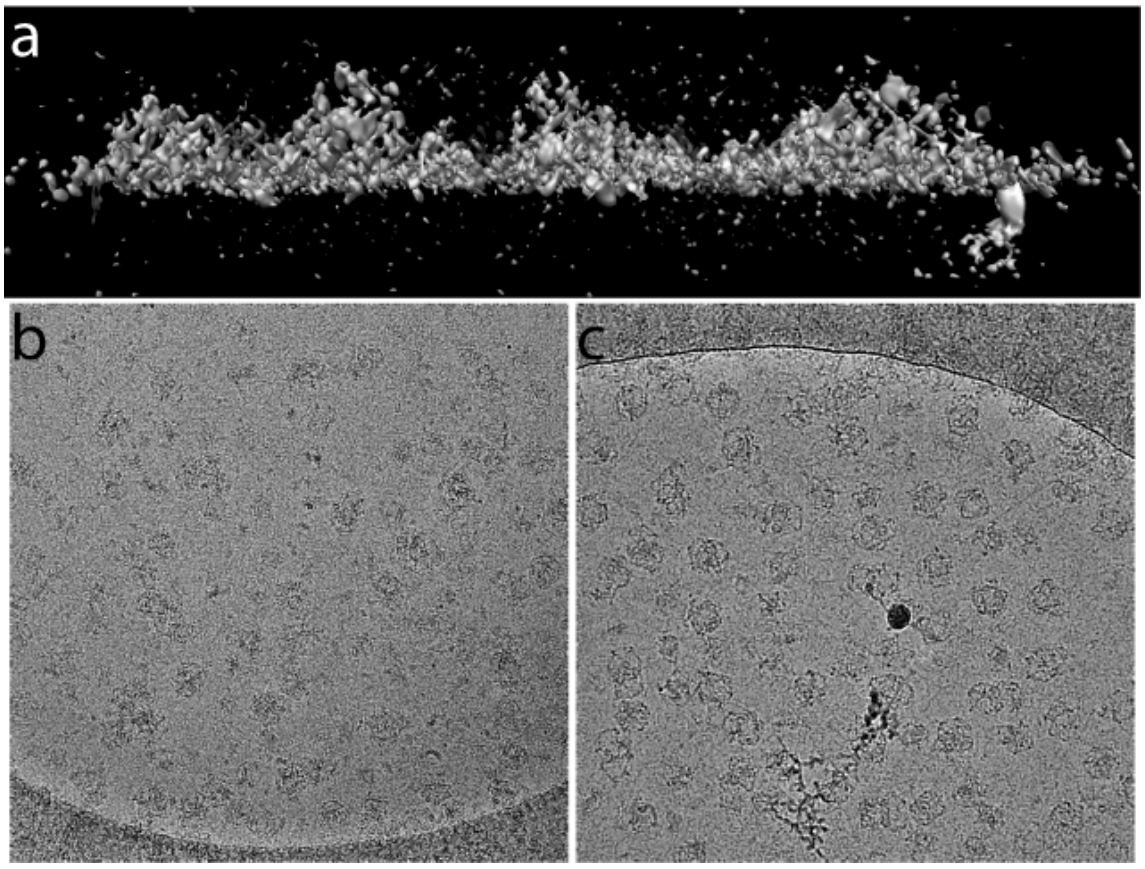

Supplementary Figure 1. Cryo-electron tomography and GRAFIX optimization of COPII cages. a) Tomogram of Sec13-31 cages viewed along the air/water interface. The tomogram shows a large amount of disordered protein at the air/water interface. The cages are obscured by the large mass of disordered protein. b) CryoEM image of cages before fixation. c) Cages after GRAFIX preparation. The cages are more distinct and featured after gradient fixation.

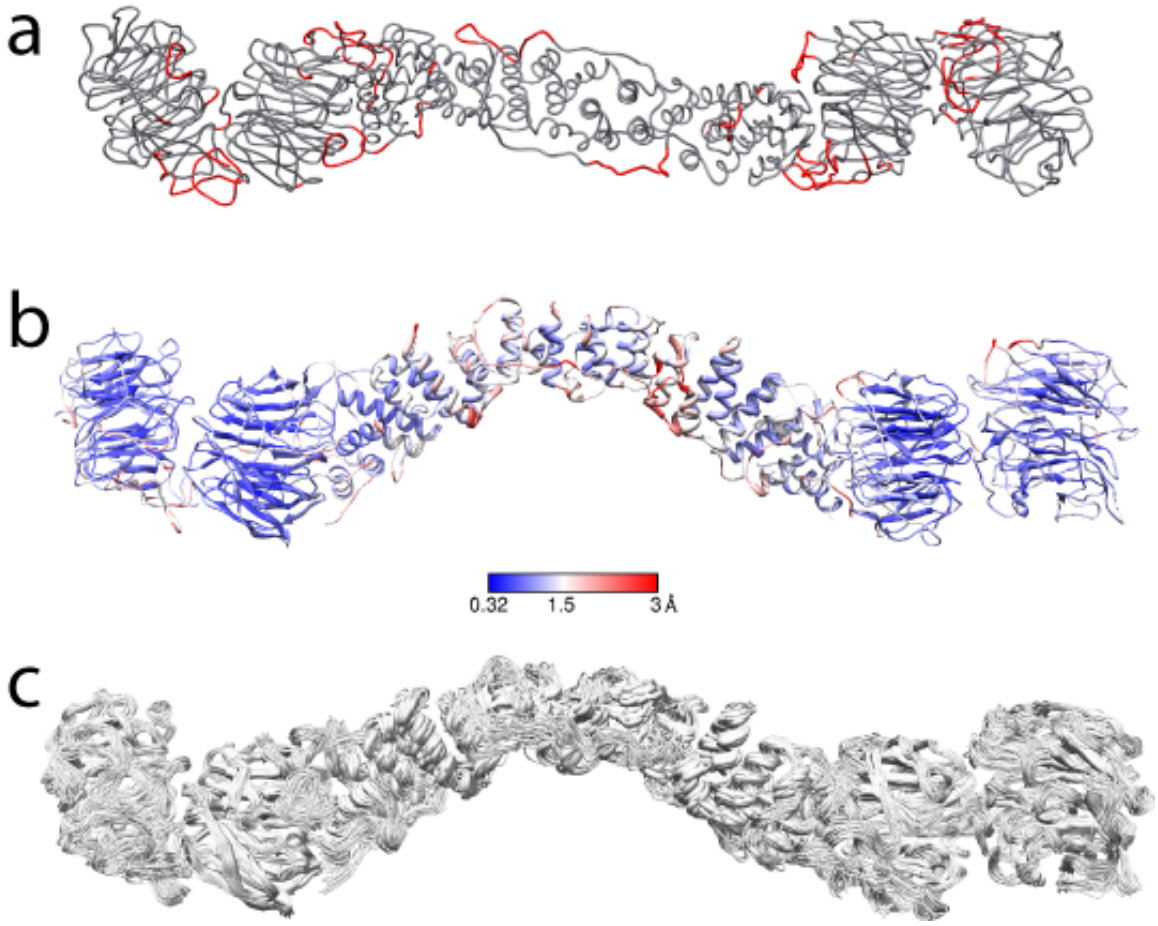

Supplementary Figure 2. Sec13-31 homology model before and after flexible fitting. a) Human homology of Sec13-31. Loops colored in red were unresolved in the yeast crystal structure and were modeled in. b) The per-atom average RMSD after symmetrically realigning the 24 flexibly fitted Sec13-31 edges mapped onto an averaged crystal structure of the edges. The mean RMSD is 1.173 Å. c) The 24 symmetrically realigned flexibly fitted Sec13-31 edges superimposed.

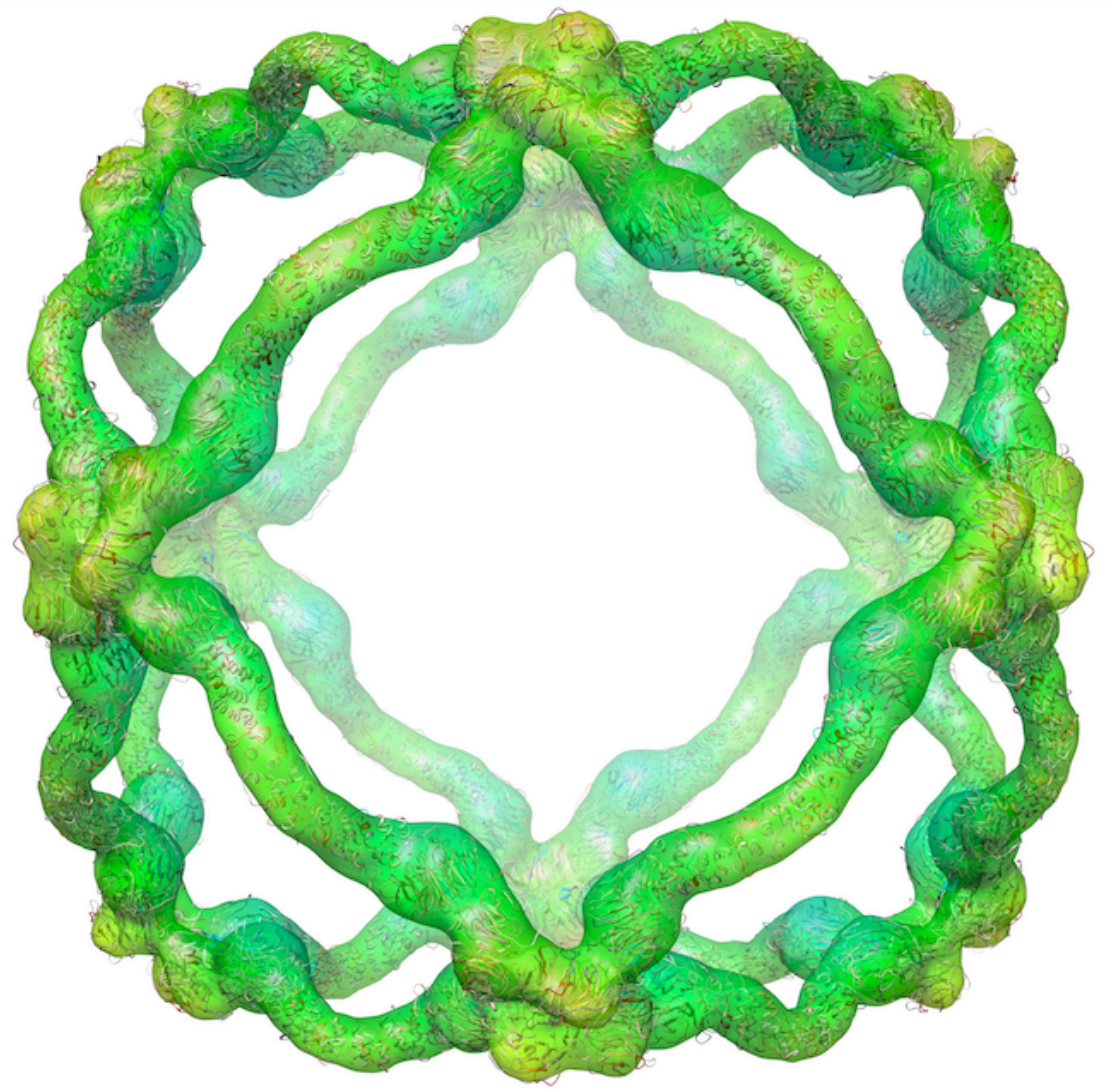

Supplementary Figure 3 12 Å reconstruction of the Sec13-31 COPII cage fitted with the pseudo-atomic structure. The cryoEM density map is radially colored. The entire flexibly fitted pseudo-atomic model of human Sec13-31 is colored as in Figure 6.

Supplementary Figure 4. See Supplemental Data file. Deuterium uptake kinetics. a) Deuterium incorporation vs. H/D exchange period (in hours) for segments of edge and cage forms of Sec31. Blue indicates edge and magenta indicates cage. b) Deuterium incorporation vs. H/D exchange period (in hours) for segments of edge and cage forms of Sec13. Blue indicates edge and magenta indicates cage.

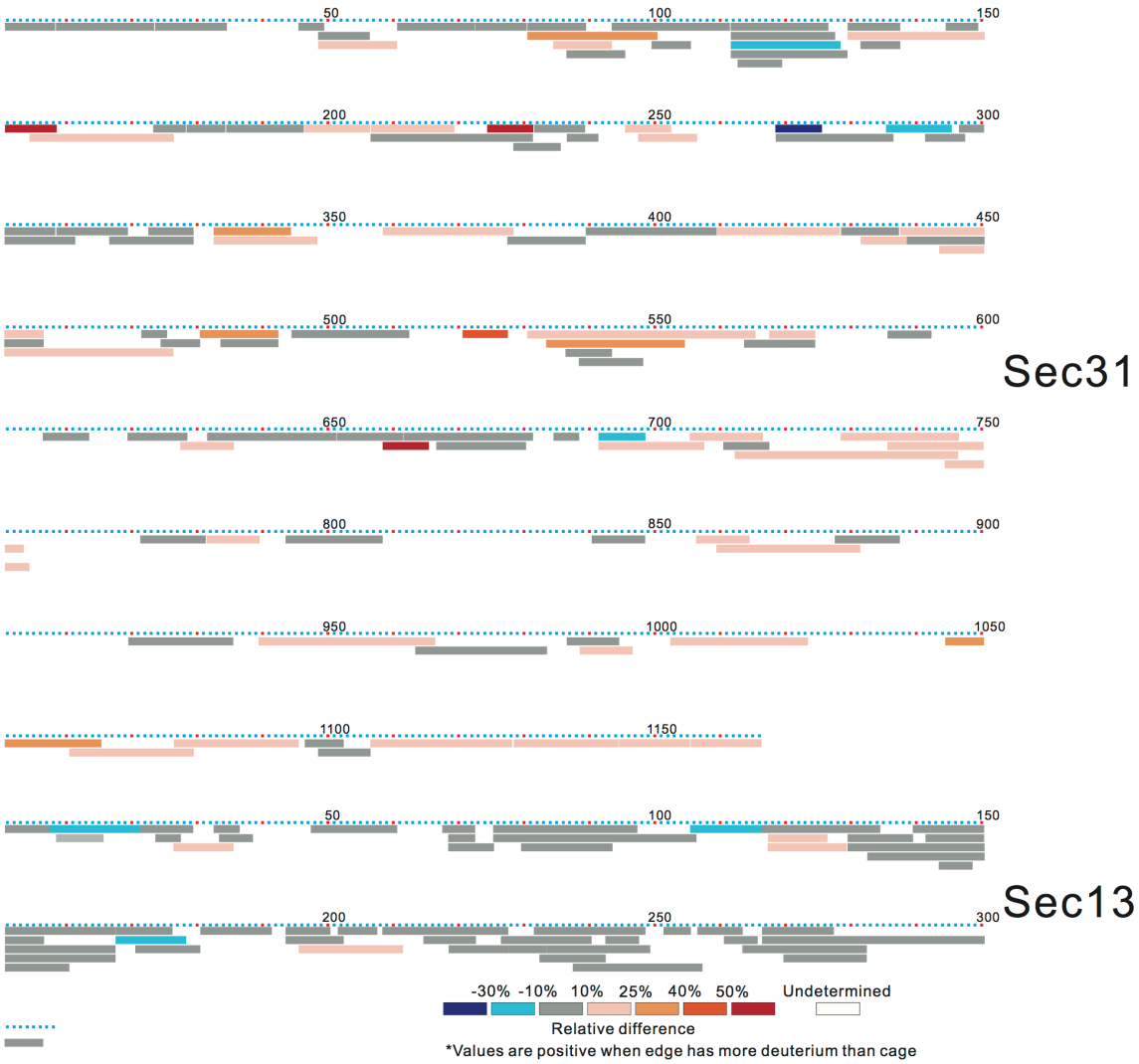

Supplementary Figure 5. Difference in deuterium uptake between Sec13-31 edge and cage, for all peptides. The deuterium uptake difference for each peptide is calculated by the ARDD method as in Fig. 6.

Supplementary Figure 6. Isotopic distributions (normalized) of peptide 439-456, showing a bimodal distribution for cage (right) but not edge (left) forms. This peptide is located in the Sec13-31 hinge region.

Supplementary Movie 1. 12 Å reconstruction of the Sec13-31 COPII cage, radially colored. The human Sec13-31 homology model, colored by chain, is then docked into the density map. An asymmetric unit of the density map is segmented out and MDFF is applied to the homology model. Octahedral symmetry is imposed when introducing 23 additional copies of the Sec13-31 atomic model. The 24 Sec13-31 atomic models are again subjected to MDFF. Multiple views of the resulting atomic model are shown at a vertex, colored as in Figure 6. At the end of the movie, an individual flexibly fitted Sec13-31 unit is shown. The two Sec13 chains are aligned, superimposed, and colored as in Figure 2. The resulting hinge with a range of 17° in the plane normal to the 4-fold axis is shown.

Supplementary Note

Flexible Fitting

The flexible fitting processes were performed by use of Molecular Dynamics Flexible Fitting (MDFF) [1]. The NAMD configuration files were created from within Visual Molecular Dynamics (VMD)[2].

MDFF uses a user-defined 3D density map to generate a grid based set of force field vectors that are proportional to the gradient of the density map. Given an atomic model that has been rigidly fit to said density map, MDFF imposes molecular dynamics simulations with the additional grid potential:

$$U_{EM}(\vec{R}) = \xi \sum_j \omega_j \begin{cases} \dfrac{1-\phi(\vec{r_j})-\phi_{thr}}{\phi_{\max}-\phi_{thr}} & \text{if } \phi(\vec{r_j}) \geq \phi_{thr}, \\ 1 & \text{if } \phi(\vec{r_j}) < \phi_{thr}. \end{cases}$$

ξ is a global scaling factor, ω_j is a per-atom scaling factor, $\phi(r_j)$ is the potential at atom j, $\phi_{\max}$ is the maximum value of $\phi(r_j)$, and ϕ_{thr} is the user-defined minimum potential threshold.

In addition, secondary structures are identified and locally restrained during the molecular dynamics simulations. The following MDFF simulations were carried out *in vacuo* at a temperature of 300 K with the scaling factor ξ= 0.3 kcal/mol and with 1 fs time steps.

The flexible fitting was done in two steps. The first step was to flexibly fit the Sec13-31 homology model to an asymmetric unit of density map. UCSF Chimera [3] was used to obtain this density map. An initial rigidly fit model of the COPII cage was made by use of the fit command in Chimera. The Color Zone feature in Chimera was used in conjunction with the initial model and the COPII cage 3D reconstruction to extract a density map consisting of one asymmetric unit. Using the fit command in Chimera, the Sec13-31 homology model was rigidly fitted to the asymmetric density map. We used MDFF to flexibly fit the rigidly fit Sec13-31 homology model to the asymmetric density map. During this process, the energy of the model was first minimized for 200 fs. The model was then subjected to the molecular dynamics simulation for 70.2 ps by use of 20 processors at FSU's High Performance Computing (HPC) cluster.

For the second step in the flexible fitting process, we used the fit and symmetry commands in Chimera to create an initial model of the COPII cage by fitting 23 additional flexibly fit asymmetric models into the COPII cage density map. To relieve potential conflicting areas at and near the 12 vertices of the COPII cage, MDFF was again used to flexibly fit this model into the COPII cage density map. The energy was first minimized for 1 ps, followed by 134.5 ps of molecular dynamics simulation by use of 72 processors of FSU's HPC cluster.

Michel Sanner's Molecular Surface (MSMS) was used to create a computational model analogous to H/D exchange [4]. The solvent-accessible surface area (SASA) was computed for a single, flexibly fit COPII vertex and for each individual Sec13-31 asymmetric unit for which the vertex is comprised. The SASA of the vertex was subtracted from the combined SASAs of the constituent asymmetric units of the vertex.

References

1. Trabuco, L. G., Villa, E., Mitra, K., Frank, J. & Schulten, K. Flexible fitting of atomic structures into electron microscopy maps using molecular dynamics. *Structure* **16,** 673-683 (2008).
2. Humphrey, W., Dalke, A. & Schulten, K. VMD: visual molecular dynamics. *J Mol Graph* **14,** 33-8, 27-8 (1996).
3. Pettersen, E. F., Goddard, T. D., Huang, C. C., Couch, G. S., *et al.* UCSF Chimera - A Visualization System for Exploratory Research and Analysis. *J. Comput. Chem.* **25,** 1605-1612 (2004).
4. Sanner, M. F., Olson, A. J. & Spehner, J. C. Reduced surface: an efficient way to compute molecular surfaces. *Biopolymers* **38,** 305-320 (1996).

Sec31			
Fragment Range by Residue ID	**Possible Reasons for HDX Difference**	**Percent Relative Difference**	**Explanation / Analysis**
50 - 60	FX	10% - 25%	This fragment is a loop on the outskirts of the WD40 domain and is found to be less flexible as part of the assembled cage.
85 - 93	FX / CC	10% - 25%	This fragment contains part of a loop and a whole β-sheet in the WD40 domain. This fragment and the next one are more flexible in the unassembled Sec13/31, possibly because they are away from the vertex contact points.
94 - 100	FX / CC	25% - 40%	This fragment contains part of a loop and most of a β-sheet in the WD40 domain.
138 - 145	PE: FX / CC and/or ME: cIII	10% - 25%	PE: This loop and β-sheet fragment is potentially being shifted by the stabilization of the 159-176 loop in the cage, causing less HDX in the cage compared to the free edges. ME: Makes contact with PE fragment 159-176.
151 - 158	FX / CC	> 50%	This fragment is part of a loop that is much more flexible in the edge than in the assembled cage. Possibly this fragment and the following fragment are flexing more in the edge than in the assembled cage.
159 - 176	cIII	10% - 25%	The PE of this loop makes contact with fragment 138-145 and possibly with its ME counterpart.
197 - 206	PE: cIII and/or ME: FX / CC	10% - 25%	This fragment is composed of a loop and a β-sheet. PE: Makes contact with lesser relative HDX loops on the ME. ME: Fragment 207-219 may be stabilizing this fragment when it connects to fragment 345-348.
207 - 219	PE: cII, cIII & cIV and/or ME: cII & cIII	10% - 25%	This loop fragment on the PE makes contact with its counterpart on the ME (cIII). Additionally: PE: Makes contact with fragment 359-378 on the ME (cIV). ME: Makes contact with fragment 359-378 on the ME (cII).
225 - 231	PE: cIII and/or ME: CC	40% - 50%	PE: Makes contact with lesser relative HDX loops on the ME. ME: Possible conformational change due to nearby contact (fragment 207-219), thereby causing this fragment in the cage

			to be less flexible than the fragment in the edge.
246 - 252	PE: cIII and/or ME: cII	10% - 25%	Each fragment in the PE and ME makes contact in one place each. Each fragment is part of a loop. PE: Makes three contacts with lesser relative HDX loops on the ME. ME: Makes contact with PE fragment 345-348 (cII).
253 - 256	FX / CC	10% - 25%	This loop fragment may become more stable in the assembled cage because of the adjacent contact fragment 246-252.
269 - 275	PE: UB / CC and/or ME: CC	< -30%	PE: This loop fragment may become unburied during cage assembly due to a conformational change. ME: This loop fragment hangs out into the space created by the increased bending of the Sec13/31 hinge in the cage versus in the edge, and is therefore more solvent accessible.
333 - 344	FX / CC	25% - 40%	This fragment, both in the PE and ME, is part of a large loop near the two WD40 domains in Sec13-31. It appears to be less flexible in the cage because of a conformational change at/near this region.
345 - 348	PE: cII and/or ME: FX / CC	10% - 25%	PE: This loop fragment makes contact with ME fragment 246-252. ME: As with fragment 333-344, this is part of a large loop and is possibly less flexible in the cage compared to in the edge.
359 - 378	PE: cII & cIV and/or ME: FX / CC	10% - 25%	PE: This loop fragment makes contact in two places - with the PE fragment 207-219 (cIV), and with the ME fragment 207-219 (cII). ME: This is a continuation of the large loop described in the previous two fragments. No vertex contacts are present.
410 - 428	CC	10% - 25%	This fragment contains the β-sheet blade connecting the α-solenoid and the Sec13 WD40 domain to Sec13. The α-solenoid portions of Sec31 in the cage appear to have more curvature than the α-solenoid in the edge. This change in conformation apparently decreases the solvent accessibility of this fragment.
432 - 438	FX / CC	10% - 25%	This loop is also a part of the connection between the α-solenoid and the Sec13

			WD40 domain. This fragment precedes an α-helix in the α-solenoid of Sec31. The conformational change that occurs in the cage appears to decrease the flexibility of this fragment.
439 - 443	FX / CC	10% - 25%	This fragment includes part of the loop connecting the α-solenoid of Sec31 with the WD40 domain of Sec13. The formation of Sec13-31 into cages reduces the flexibility of this fragment.
444 - 471	CC / B	10% - 25%	This large fragment contains a two small α-helices and part of another. This fragment is part of the proposed hinge region between Sec13 and the α-solenoid region of Sec31.
481 - 492	CC / B	25% - 40%	This fragment contains an α-helix and a part of another α-helix. This fragment immediately precedes a long outstretched loop involved in the dimerization of Sec31 in the curve. In the cage this fragment may become more buried because of the conformational change in the curvature of the edge.
521 - 527	FX / CC / B	40% - 50%	This fragment is a part of a much longer loop. The large decrease in HDX from the edge to the cage may be explained by hypothesizing that this fragment becomes partially buried due to the conformational change of the curved edge.
531 - 533	FX / CC	10% - 25%	This fragment is part of the first α-helix following the long Sec31 dimerization loop. It is likely that the added curvature of the cage versus the edge reduces its flexibility by rigidifying the curved edge.
534 - 554	FX / CC / B	25% - 40%	This fragment contains almost two α-helices. It is likely that the added curvature of the cage versus the edge reduces its flexibility by rigidifying the curved edge.
568 - 574	FX / CC / B	10% - 25%	This fragment is a loop that almost has the structure of an α-helix. It is likely that the added curvature of the cage versus the edge reduces its flexibility by rigidifying the curved edge.
629 - 635	CC / B	10% - 25%	This fragment is part of an α-helix in the α-solenoid. It is likely that the change in curvature between the cage and the edge causes this fragment to become buried as the α-helices become more

			packed.
662 - 665	CC / B	> 50%	This fragment is part of an α-helix in the α-solenoid that is much less solvent accessible in the cage than in the edge. It is likely that the change in curvature between the cage and the edge causes this fragment to become buried as the α-helices become more packed. Most of the α-helix associated with this fragment is wedged between three adjacent α-helices in our current model, which could explain the large difference in relative HDX.
699 - 707	FX / CC / B	10% - 25%	Most of this fragment is part of a larger loop. The loop apparently becomes more packed into the edge in the assembled cage compared to the unassembled edge.
708 - 712	FX / CC / B	10% - 25%	This fragment is part of an α-helix in the α-solenoid. This fragment is approaching the proposed hinge area between Sec13 and Sec31 and thus the relative difference in HDX may be caused by the flexibility of the hinge and/or this fragment being buried within the α-solenoid in the cage versus the edge.
713 - 746	FX / CC / B	10% - 25%	This large fragment contains α-helices and connecting loops in the α-solenoid. This fragment is part of the proposed hinge area between Sec13 and Sec31 and thus the relative difference in HDX may be caused by the flexibility of the hinge and/or this fragment being buried within the α-solenoid in the cage versus the edge.
747 - 753	FX	10% - 25%	This small loop fragment contains the C-terminus of Sec31, which resides at the hinge interface. The decrease in HDX from the cage to the edge may be related to the proposed hinge behavior between Sec13 and Sec31.

Sec13			
Fragment Range by Residue ID	**Possible Reasons for HDX Difference**	**Percent Relative Difference**	**Explanation / Analysis**
44 - 46	FX	10% - 25%	This fragment is a loop connecting two particularly floppy β-sheets.
139 - 143	FX	10% -	The β-sheet contained in this fragment is

		25%	nearly perpendicular to the β-barrel and is on the outskirts of the β-barrel.
156 - 170	FX	10% - 25%	This fragment is a portion of a long loop on the outskirts of the β-barrel.
215 - 225	B	10% - 25%	The β-sheet in this fragment is likely more buried in the assembled cage than in the unassembled edge.

Supplementary Table 1. Relative difference in HDX between the unassembled Sec13/31 edge and the assembled COPII cage for all HDX fragments. Positive percent relative difference values indicate a fragment that underwent greater HDX in the edge than in the cage. CC, Conformational Change; FX, Flexibility; B, Buried; UB, Unburied; ME, Minus End; PE, Positive End.